Steady-state Stability Assessment of AC-busbar Plug-in Electric Vehicle Charging Station with Photovoltaic

Rui Wang, *Student Member*, *IEEE*, Qiuye Sun, *Senior Member*, *IEEE*, Dehao Qin, *Student Member*, *IEEE*, Yushuai Li, *Member*, *IEEE*, Xiangke Li, and Peng Wang, *Fellow*, *IEEE*

***Abstract*—Although the deployment of alternating current (AC) -busbar plug-in electric vehicle (PEV) charging station with photovoltaic (PV) is a promising alternative, the interaction among subsystems always causes the instability problem. Meanwhile, the conventional generalized Nyquist criterion (GNC) is complex, and it is not suitable for the design of the AC system. Therefore, this paper proposes a modified infinity-one-norm (MION) stability criterion based on the impedance method to assess the stability of the foresaid charging station. Firstly, the typical structure and operation modes of the charging station are studied. Furthermore, each subsystem impedance matrix is built by small-signal method, and the MION stability criterion based on impedance method is proposed to assess the charging station stability. Compared with the previous simplified stability criteria based on the norm, the proposed criterion has lower conservatism. Furthermore, the design regulation for the controller parameters is provided, and the stability recovery way is provided by connecting the doubly-fed line and energy storage equipment, which are selected based on intermediate variable, i.e., short-circuit ratio (SCR). Finally, the effectiveness and conservatism of the proposed stability criterion are validated through simulation and experimental results.**

***Index Terms*—impedance-norm, plug-in electric vehicle (PEV), charging station, photovoltaic (PV), stability assessment.**

Manuscript received: March 23, 2020; accepted: July 3, 2020. Date of Cross-Check: July 3, 2020. Date of online publication: Stptember 9, 2020.

This work was supported by National Key Research and Development Program of China (No. 2018YFA0702200), National Natural Science Foundation of China (No. 61773109), and Major Program of National Natural Foundation of China (No. 61573094).

R. Wang, Q. Sun (corresponding author), and D. Qin are with the College of Information Science and Engineering, Northeastern University, Shenyang 110819, China, and R. Wang is also with the School of Electrical and Electronic Engineering, Nanyang Technological University, 639798, Singapore (e-mail: 1610232@stu.neu.edu.cn; sunqiuye@ise.neu.edu.cn; mattqin1216@outlook.com).

Y. Li is with the Department of Electrical and Computer Engineering, University of Denver, Denver, 80208 Colorado, USA (e-mail: lysise@126.com).

X. Li is with the Northwestern Polytechnical University, Xi'an, 710072, China, and he is also with the School of Electrical and Electronic Engineering, Nanyang Technological University, 639798, Singapore (e-mail: N1906398J@e.ntu.edu.sg).

P. Wang is with the School of Electrical and Electronic Engineering, Nanyang Technological University, 639798, Singapore (e-mail: epwang@ntu.edu.sg).

DOI: 10.35833/MPCE.2020.000182

I. Introduction

RECENTLY, the increasing pressure from energy and environment protection has made the research for advanced energy infrastructures urgent. As an advanced power energy infrastructure, the plug-in electric vehicle (PEV) has been regarded as an environmentally friendly vehicle with high potential to reduce fuel consumption and CO_2 emissions [1]. However, since the PEV needs to be connected to the main grid for absorbing energy, the advantages of the PEV are not obvious due to the indirect fuel consumption and CO_2 emissions [2]. With the rapid development of solar energy resources, the AC-busbar PEV charging station with photovoltaic (PV) has become an attractive choice [3]. Compared with the conventional power system, the stability of the AC-busbar PEV charging station with PV has been seriously threatened due to the negative-damping, low-inertia and negative-impedance nature of the converter-dominated systems [4]. Therein, the steady-state instability problems are critical issues in electromagnetic timescale shown in Fig. A1 in Appendix A [5]. Thus, this paper focuses on the impedance-norm-based stability assessment of the AC-busbar PEV charging station with PV in electromagnetic timescale.

At present, two main architectures of public charging stations are defined in the Danish EDISON project, i.e., the AC-busbar charging station and DC-busbar charging station [3]. Meanwhile, PEVs are divided into two main categories, i.e., the PEV with vehicle-to-grid (V2G) concept and the conventional PEV [6]. In real system, the conventional PEV still occupies the dominant position such that only the charging station consisting of the conventional PEV is considered in this paper. Although the research regarding PEV charging station with PV focuses more on charging strategies or energy management [7], [8], the stability assessment of the PEV charging station with PV is also an important issue. Reference [9] first proposes the impedance-based stability criterion by utilizing measured data to assess the stability of DC-busbar PEV charging station with PV and applying a two-port small-signal model. Nevertheless, the impedance-norm-based stability assessment for the AC-busbar PEV charging station with PV is not studied in electromagnetic timescale.

Two main stability assessment approaches are studied for the stability analysis and design of the controller parameters

of the system dominated by power electronic converters, i.e., state-space-based approach and impedance-based approach. For the state-space-based approach, [10] proposes a small-signal stability approach based on state-space model without the voltage/current double closed loop controller for parallel-connected converters. Reference [11] further proposes a full-order state-space model. Meanwhile, the computation burden of the system with multiple converters is heavy [11], [12]. To reduce the computation burden, model order reduction methods, such as the singular perturbations method [12] and the participation analysis [13], have been applied to study the stability issues. Nevertheless, the state-space-based approach requires the detailed internal control information of each converter, which is not convenient to obtain in real applications. Besides, it is difficult to establish the state-space function of the complex power system [10]. Based on this, the impedance-based approach has been widely used for cascaded systems [14]. Therein, the impedance-based approach on the basis of the ratio between the impedances of two subsystems at the interface, has plenty of potential advantages to explicitly explain the impact of individual subsystems on the system stability assessment [14]. Moreover, this approach is more concerned with the interactive stability of the grid-connected inverter and main grid, and the stability analysis of the whole system consisting of multiple converters.

To sum up, the impedance-based approach is suitable for the stability assessment of the charging station. Furthermore, it is significant to check the right-half-plane (RHP) poles of the transfer function matrix while using the generalized Nyquist criterion (GNC). The inverse Nyquist stability criterion is proposed to make sure that the poles at origin and RHP of the inverter output impedance could be ignored [15]. To solve the bidirectional power flow, the sum type criterion is first proposed in [16]. Furthermore, from the viewpoint of different applications regarding the impedance-based approach, a stability assessment is proposed for the high-voltage direct current (HVDC) systems [17], and an impedance-based stability criterion is proposed to assess the stability of the DC-busbar PEV charging station with PV [8]. However, the above-mentioned methods are complex and unsuitable for the design of the AC system [18]. To solve the disadvantage of complicated calculation, several simplified stability assessment criteria based on impedance specifications are proposed for AC/DC systems [18]-[21]. Therein, the D-channel criterion indicates that the stability of the DC systems could be decided through source subsystem and load subsystem [20]. However, this criterion could not provide sufficient conditions to assess the stability in AC systems. Furthermore, the singular-value criterion indicates that the system stability would be ensured if the arithmetic product of the maximum singular-values is less than one over the entire frequency range [21]. To further simplify the calculation, the impedance-norm-based criteria are proposed to assess the stability of AC systems. According to the difference of the norm style and the arithmetic product range, the impedance-norm based criteria could be divided into three categories, i.e., the G-norm (GN) criterion [19], the infinity-norm (IN) criterion [19], and the infinity-one-norm (ION) criterion [18]. The detailed identification conditions are found in Table AI in Appendix A. Undeniably, the conservatism would be introduced in the foresaid simplified criteria.

To accurately assess the stability of AC-busbar PEV charging station with PV, this paper proposes an MION stability criterion based on the impedance method. The main features and benefits of this paper are listed as follows.

1) This paper proposes an MION stability criterion based on impedance method to assess the stability of AC-busbar PEV charging station with PV in electromagnetic timescale. Compared with the GN criterion [19], the ION criterion [19] and the IN criterion [18], the proposed MION stability criterion has lower conservatism.

2) Based on the proposed stability criterion, the design regulation for the controller parameters is provided, and the stability recovery ways are provided by connecting the doubly-fed line and energy storage equipment, which are selected based on intermediate variable, i. e., short-circuit ratio (SCR).

The rest of this paper is organized as follows. The typical structure and operation modes of AC-busbar PEV charging station with PV are analyzed in Section II. Subsequently, each subsystem impedance matrix and the MION stability criterion based on impedance method are proposed to assess the stability of the charging station in Section III. In Section IV and Section V, the proposed stability assessment is validated through extensive simulation and hardware results. Finally, the conclusion is obtained in Section VI.

II. Typical Structure and Operation Modes of AC-busbar PEV Charging Station with PV

As shown in Fig. 1, the AC-busbar PEV charging station with PV is defined in the Danish EDISON project [3]. To simplify stability analysis, the typical standalone PV-PEV charging station is simplified as Fig. 2, where PCC is the point of common coupling. Thereinto, the PEV adopts the conventional constant voltage charging mode. In this charging station, the source inverter delivers solar energy from the PV to the AC bus. The rectifier converts the energy from the AC bus to PEV. Meanwhile, the main grid provides voltage and frequency regulation. According to the amount of power supplied by the PV arrays and power absorbed by the PEV, the typical standalone PV-PEV charging station has four possible operation modes. P_{PV}, P_{PEV} and P_g are the supplied power of the PV, the absorbed power of the PEV, and the supplied/absorbed power of the main grid, respectively. The detailed operation modes of the typical standalone PV-PEV charging station can be described as follows.

1) Operation mode 1: If $P_{PV}=0$, the absorbed power of the PEV is provided only by the main grid, and the PV is shut down, i.e., $P_{PEV}=P_g$. Thus, the main grid is the source subsystem, and the PEV is the load subsystem.

2) Operation mode 2: If $0<P_{PV}<P_{PEV}$, the absorbed power of the PEV is provided by the main grid and the PV, i.e., $P_{PEV}=P_g+P_{PV}$. Thus, both the main grid and the PV are the source subsystems, and the PEV is the load subsystem.

3) Operation mode 3: If $P_{PV}=P_{PEV}$, the absorbed power of the PEV is only provided by the PV, and the main grid is

shut down, i.e., $P_{PEV}=P_{PV}$. Thus, the PV is the source subsystem, and the PEV is the load subsystem.

4) Operation mode 4: If $P_{PV}>P_{PEV}$, the absorbed power of the PEV is only provided by the PV, and the excessive solar power is used to feed the main grid, i. e., $P_{PEV}=P_{PV}-P_g$. Thus, the PV is source subsystem, and both the main grid and the PEV are load subsystems.

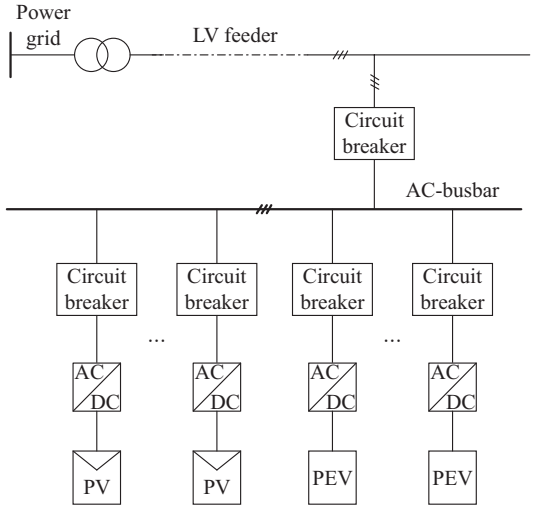

Fig. 1. Typical structure of AC-busbar EV charging station with PV.

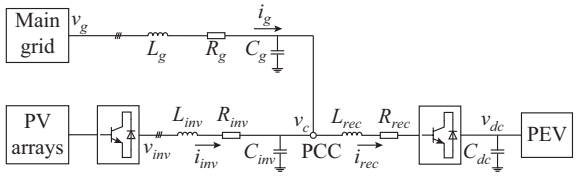

Fig. 2. Typical standalone PV-PEV charging station.

III. MINO Stability Criterion Based on Impedance Method for AC-busbar PEV Charging Station with PV

In this section, each subsystem impedance model based on small-signal linearization is built in *d-q* frame. The MINO stability criterion based on impedance method is proposed to assess the stability of the AC-busbar PEV charging station with PV in electromagnetic timescale. Eventually, the controller parameters and stability analysis are provided.

A. Impedance Model of PEV

The interface converter of the PEV is controlled by the traditional double-loop current/voltage controller, which is shown in Fig. 3. Thereinto, the phase-locked-loop (PLL) is always used to obtain the three-phase angular speed of the rotating *d-q* frame. Under steady-state conditions, the three-phase space-phasor angular speed is described as follows.

$$\omega = G_{PLL}(s)V_{cq} \tag{1}$$

where G_{PLL} is the PLL proportional-integral (PI) controller; s is the Laplace operator; V_c is the AC voltage in AC-link capacitor; and the subscripts d and q mean the *d-q* components, respectively. The dynamic model of the voltage-source rectifier can be represented on the *d-q* frame by:

$$V_{cd} = sI_{recd}L_{rec} - \omega I_{recq}L_{rec} + D_d V_{dc} \tag{2}$$

$$V_{cq} = sI_{recq}L_{rec} + \omega I_{recd}L_{rec} + D_q V_{dc} \tag{3}$$

$$sC_{dc}V_{dc} + I_{dc} = 1.5\left(D_d I_{recd} + D_q I_{recq}\right) \tag{4}$$

$$V_{dc} = I_{dc}R_{load} \tag{5}$$

where I_{rec} is the rectifier input AC current; L_{rec} is the equivalent inductance of the AC filter; D is the rectifier duty ratio; V_{dc} is the rectifier output DC voltage; C_{dc} is the rectifier output DC capacitor; R_{load} is the terminated load; and ω is the angular speed.

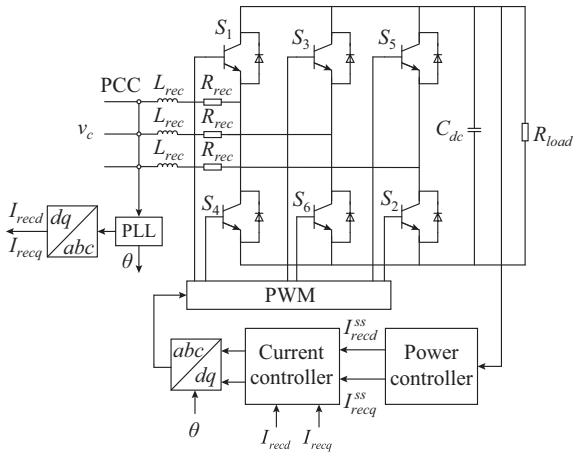

Fig. 3. Controller architecture of PEV.

The classical PI-based voltage controller and PI-based current controller are applied to (2) and (3) for the tracking and regulation of DC voltage. Thus, the steady-state value of the controlled signals is shown as follows.

$$I_{recd}^{ss} = \left(V_{dc}^{ss} - V_{dc}\right)G_v^{rec}(s) \tag{6}$$

$$I_{recq}^{ss} = 0 \tag{7}$$

$$D_d V_{dc} = -\left(I_{recd}^{ss} - I_{recd}\right)G_i^{rec}(s) + V_{cd} + \omega L_{rec} I_{recq} \tag{8}$$

$$D_q V_{dc} = -\left(I_{recq}^{ss} - I_{recq}\right)G_i^{rec}(s) + V_{cq} - \omega L_{rec} I_{recd} \tag{9}$$

where $G_v^{rec}(s)$ and $G_i^{rec}(s)$ are the voltage and current inner loop controllers, respectively; and the superscript *ss* means the steady-state value. Using the small-signal perturbations on (1)-(3), the small-signal modeling of (2) and (3) are represented by (10) and (11), respectively, where Δ represents small disturbance.

$$\begin{aligned}\Delta V_{cd} = {} & sL_{rec}\Delta I_{recd} - G_{PLL}(s)L_{rec}V_{cq}^{ss}\Delta I_{recq} + \\ & D_d^{ss}\Delta V_{dc} + \Delta D_d V_{dc}^{ss} - G_{PLL}(s)L_{rec}\Delta V_{cq} I_{recq}^{ss}\end{aligned} \tag{10}$$

$$\begin{aligned}\Delta V_{cq} = {} & sL_{rec}\Delta I_{recq} + G_{PLL}(s)L_{rec}V_{cq}^{ss}\Delta I_{recd} + \\ & D_q^{ss}\Delta V_{dc} + \Delta D_q V_{dc}^{ss} + G_{PLL}(s)L_{rec}\Delta V_{cq} I_{recd}^{ss}\end{aligned} \tag{11}$$

In order to elicit the input admittance matrix in a rotating reference frame, (10) and (11) can be rewritten as:

$$\begin{aligned}\left[A_1\right]_{2\times 2}\begin{bmatrix}\Delta V_{cd}\\ \Delta V_{cq}\end{bmatrix} = {} & \left[A_2\right]_{2\times 2}\begin{bmatrix}\Delta I_{recd}\\ \Delta I_{recq}\end{bmatrix} + \left[A_4\right]_{2\times 1}\Delta V_{dc} + \\ & \left[A_3\right]_{2\times 2}\begin{bmatrix}\Delta D_d\\ \Delta D_q\end{bmatrix}\end{aligned} \tag{12}$$

where $\left[A_1\right]_{2\times2}=\begin{bmatrix}1 & G_{PLL}(s)L_{rec}I_{recq}^{ss}\\ 0 & 1-G_{PLL}(s)L_{rec}I_{recd}^{ss}\end{bmatrix}$, $\left[A_2\right]_{2\times2}=\begin{bmatrix}sL_{rec} & -G_{PLL}(s)L_{rec}V_{cq}^{ss}\\ G_{PLL}(s)L_{rec}V_{cq}^{ss} & sL_{rec}\end{bmatrix}$, $\left[A_3\right]_{2\times2}=\begin{bmatrix}V_{dc}^{ss} & 0\\ 0 & V_{dc}^{ss}\end{bmatrix}$, $\left[A_4\right]_{2\times1}=\begin{bmatrix}D_d^{ss} & D_q^{ss}\end{bmatrix}^{\mathrm{T}}$.

In a similar analysis, the small-signal modeling from (5) to (9) is represented as:

$$\Delta V_{dc}=\left[A_5\right]_{1\times2}\begin{bmatrix}\Delta I_{recd}\\ \Delta I_{recq}\end{bmatrix}+\left[A_6\right]_{1\times2}\begin{bmatrix}\Delta D_d\\ \Delta D_q\end{bmatrix} \tag{13}$$

$$\begin{bmatrix}\Delta D_d\\ \Delta D_q\end{bmatrix}=\left[A_7\right]_{2\times2}\begin{bmatrix}\Delta I_{recd}\\ \Delta I_{recq}\end{bmatrix}+\left[A_8\right]_{2\times2}\begin{bmatrix}\Delta V_{cd}\\ \Delta V_{cq}\end{bmatrix}+\left[A_9\right]_{2\times1}\Delta V_{dc} \tag{14}$$

where $\left[A_5\right]_{1\times2}=\begin{bmatrix}\frac{1.5D_d^{ss}R_{load}}{C_{dc}R_{load}s+1} & \frac{1.5D_d^{ss}R_{load}}{C_{dc}R_{load}s+1}\end{bmatrix}$, $\left[A_6\right]_{1\times2}=\begin{bmatrix}\frac{1.5I_{recd}^{ss}R_{load}}{C_{dc}R_{load}s+1} & \frac{1.5I_{recd}^{ss}R_{load}}{C_{dc}R_{load}s+1}\end{bmatrix}$, $\left[A_7\right]_{2\times2}=\frac{1}{V_{dc}^{ss}}\begin{bmatrix}G_i(s) & \omega^{ss}L_{rec}\\ -\omega^{ss}L_{rec} & G_i(s)\end{bmatrix}$, $\left[A_8\right]_{2\times2}=\begin{bmatrix}\frac{1-G_v(s)G_i(s)}{V_{dc}^{ss}} & \frac{G_{PLL}(s)L_{rec}I_{recq}^{ss}}{V_{dc}^{ss}}\\ 0 & \frac{1-G_{PLL}(s)L_{rec}I_{recd}^{ss}}{V_{dc}^{ss}}\end{bmatrix}$, $\left[A_9\right]_{2\times1}=\frac{1}{V_{dc}^{ss}}\left[G_v(s)G_i(s)-D_d^{ss}\quad -D_d^{ss}\right]^{\mathrm{T}}$.

By substituting (13) into (12), (15) is obtained as:

$$\left[A_1\right]_{2\times2}\begin{bmatrix}\Delta V_{cd}\\ \Delta V_{cq}\end{bmatrix}=\left(\left[A_1\right]_{2\times2}+\left[A_4\right]_{2\times1}\left[A_5\right]_{1\times2}\right)\begin{bmatrix}\Delta I_{recd}\\ \Delta I_{recq}\end{bmatrix}+\left(\left[A_3\right]_{2\times2}+\left[A_4\right]_{2\times1}\left[A_6\right]_{1\times2}\right)\begin{bmatrix}\Delta D_d\\ \Delta D_q\end{bmatrix} \tag{15}$$

By substituting (13) into (14), (16) is obtained as:

$$\left(\left[1\right]_{2\times2}-\left[A_9\right]_{2\times1}\left[A_6\right]_{1\times2}\right)\begin{bmatrix}\Delta D_d\\ \Delta D_q\end{bmatrix}=\left[A_8\right]_{2\times2}\begin{bmatrix}\Delta V_{cd}\\ \Delta V_{cq}\end{bmatrix}+\left(\left[A_1\right]_{2\times2}+\left[A_9\right]_{2\times1}\left[A_5\right]_{1\times2}\right)\begin{bmatrix}\Delta I_{recd}\\ \Delta I_{recq}\end{bmatrix} \tag{16}$$

By removing $\left[\Delta D_d\quad \Delta D_q\right]^{\mathrm{T}}$, the input admittance matrix can be obtained as:

$$\begin{aligned}\boldsymbol{Y}_{PEVin}&=\begin{bmatrix}Y_{PEVdd} & Y_{PEVdq}\\ Y_{PEVqd} & Y_{PEVqq}\end{bmatrix}=\\ &\left\{\left(\left[A_4\right]\left[A_6\right]+\left[A_3\right]\right)\left(\left[1\right]-\left[A_9\right]\left[A_6\right]\right)^{-1}\times\right.\\ &\left(\left[A_7\right]+\left[A_9\right]\left[A_5\right]\right)+\left[A_4\right]\left[A_5\right]+\left[A_2\right]\rangle\times\\ &\left.\left[A_1\right]-\left(\left[A_4\right]\left[A_6\right]+\left[A_3\right]\right)\left(\left[1\right]-\left[A_9\right]\left[A_6\right]\right)^{-1}\left[A_8\right]\right\}\end{aligned} \tag{17}$$

B. Impedance Model of PV

The stability assessment results indicate that the grid-connected inverter controlled by the *P-Q* controller is prone to losing stability, whereas the inverters controlled by the droop controller still work well under an ultra-weak main grid or with a large number of inverters connected to the charging station. Of course, previous literatures have also been proposed in this case. For example, [22] proposes a novel integral barrier Lyapunov function (BLF) based controller combined with the L'Hospital's rule, which is first applied to switched nonlinear systems. Reference [23] proposes a novel common-mode voltage suppression method based on the complementary modulation sequence. Meanwhile, the inverter controlled by the droop controller is more suitable for achieving high penetration of solar energy generation from the viewpoint of the charging station stability [4]. Figure 4 shows the typical control structure of the voltage-source inverter controlled by droop control. The current and voltage dynamics model of this controller in the *d-q* frame is shown as:

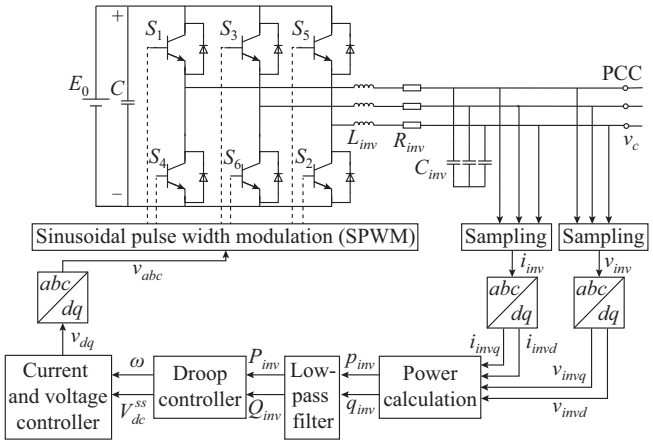

Fig. 4. Controller architecture of PV.

$$V_{invd}=I_{invd}\left(R_{inv}+sL_{inv}\right)-\omega L_{inv}I_{invq}+V_{cd} \tag{18}$$

$$V_{invq}=I_{invq}\left(R_{inv}+sL_{inv}\right)+\omega L_{inv}I_{invd}+V_{cq} \tag{19}$$

$$I_{invd}=C_{inv}V_{cd}s-\omega C_{inv}V_{cq}+I_{cd} \tag{20}$$

$$I_{invq}=C_{inv}V_{cq}s+\omega C_{inv}V_{cd}+I_{cq} \tag{21}$$

where V_{invd}, V_{invq}, I_{invd}, and I_{invq} are the inverter output voltages and currents in the *d-q* frame, respectively; V_{cd}, V_{cq}, I_{cd}, and I_{cq} are the inverter voltages and currents in the *d-q* frame, respectively; and R_{inv}, L_{inv}, and C_{inv} are the resistance, inductance, and capacitance, respectively. The voltage and current double loop controller can be represented as:

$$I_{invd}^{ss}=G_v^{inv}\left(V_{cd}^{ss}-V_{cd}\right)-\omega C_{inv}V_{cq}+KI_{cd} \tag{22}$$

$$I_{invq}^{ss}=G_v^{inv}\left(V_{cq}^{ss}-V_{cq}\right)+\omega C_{inv}V_{cd}+KI_{cq} \tag{23}$$

$$V_{invd}^{ss}=G_i^{inv}\left(I_{cd}^{ss}-I_{cd}\right)-\omega L_{inv}I_{cq}+V_{cd} \tag{24}$$

$$V_{invq}^{ss}=G_i^{inv}\left(I_{cq}^{ss}-I_{cq}\right)+\omega L_{inv}I_{cd}+V_{cq} \tag{25}$$

where I_{cd}^{ss}, I_{cq}^{ss}, V_{cd}^{ss}, and V_{cq}^{ss} are the inverter current and voltage signals in the *d-q* frame, respectively; $G_i^{inv}=k_{ip}^{inv}+k_{ii}^{inv}/s$ and $G_v^{inv}=k_{vp}^{inv}+k_{vi}^{inv}/s$ are the current and voltage double-loop PI controllers, respectively, k_{ip}^{inv}, k_{ii}^{inv}, k_{vp}^{inv}, and k_{vi}^{inv} are the PI controller parameters; and K is a feed-forward gain. Additionally, the instantaneous active power p_{inv} and reactive power q_{inv} can be given by (26), and the inner controllers of the inverter need to provide active or passive damping for possible oscillations between the output filters of the inverters and the transmission line. Thus, a low-pass filter should be

applied to the inverter, and the active and reactive output power P_{inv} and Q_{inv} can be obtained by (27).

$$p_{inv}=1.5\left(V_{cd}I_{cd}+V_{cq}I_{cq}\right) \tag{26}$$

$$q_{inv}=1.5\left(V_{cd}I_{cq}-V_{cq}I_{cd}\right) \tag{27}$$

$$P_{inv}=\frac{\omega_f}{s+\omega_f}p_{inv} \tag{28}$$

$$Q_{inv}=\frac{\omega_f}{s+\omega_f}q_{inv} \tag{29}$$

where ω_f is the cutoff frequency of the low-pass filter. The droop controller can be represented as [22]:

$$\omega=\omega^{ss}-mP_{inv} \tag{30}$$

$$V_{cd}^{ss}=V^{ss}-nQ_{inv} \tag{31}$$

where ω^{ss} and V^{ss} are the rated angle speed and voltage, respectively. Using small perturbations on (18), (19), (24) and (25), and dynamic phase method [23], the small-signal model of ΔI_{inv}^{ss} can be represented by:

$$\begin{bmatrix}\Delta I_{invd}^{ss}\\ \Delta I_{invq}^{ss}\end{bmatrix}=\left[B_1\right]_{2\times2}\begin{bmatrix}\Delta I_{invd}\\ \Delta I_{invq}\end{bmatrix}+\left[B_2\right]_{2\times2}\begin{bmatrix}\Delta\omega\\ \Delta V_{cd}^{ss}\end{bmatrix} \tag{32}$$

where $\left[B_1\right]_{2\times2}=\begin{bmatrix}\dfrac{R_{inv}+sL_{inv}+G_i^{inv}(s)}{G_i^{inv}(s)} & 0\\ 0 & \dfrac{R_{inv}+sL_{inv}+G_i^{inv}(s)}{G_i^{inv}(s)}\end{bmatrix}$,

$\left[B_2\right]_{2\times2}=\begin{bmatrix}-\dfrac{I_{invq}^{ss}L_{inv}}{G_i^{inv}(s)} & 0\\ \dfrac{I_{invd}^{ss}L_{inv}}{G_i^{inv}(s)} & 0\end{bmatrix}$.

Utilizing small perturbations on (20)-(23) yields:

$$\begin{bmatrix}\Delta I_{invd}\\ \Delta I_{invq}\end{bmatrix}=\begin{bmatrix}\Delta I_{cd}\\ \Delta I_{cq}\end{bmatrix}+\left[B_3\right]_{2\times2}\begin{bmatrix}\Delta V_{cd}\\ \Delta V_{cq}\end{bmatrix}+\left[B_4\right]_{2\times2}\begin{bmatrix}\Delta\omega\\ \Delta V_{cd}^{ss}\end{bmatrix} \tag{33}$$

$$\begin{bmatrix}\Delta I_{invd}^{ss}\\ \Delta I_{invq}^{ss}\end{bmatrix}=\left[B_5\right]_{2\times2}\begin{bmatrix}\Delta V_{cd}\\ \Delta V_{cq}\end{bmatrix}+\left[B_6\right]_{2\times2}\begin{bmatrix}\Delta I_{cd}\\ \Delta I_{cq}\end{bmatrix}+\left[B_7\right]_{2\times2}\begin{bmatrix}\Delta\omega\\ \Delta V_{cd}^{ss}\end{bmatrix} \tag{34}$$

where $\left[B_3\right]_{2\times2}=\begin{bmatrix}sC_{inv} & -\omega^{ss}C_{inv}\\ \omega^{ss}C_{inv} & sC_{inv}\end{bmatrix}$, $\left[B_4\right]_{2\times2}=\begin{bmatrix}0 & 0\\ V_{cd}^{ss}C_{inv} & 0\end{bmatrix}$,

$\left[B_5\right]_{2\times2}=\begin{bmatrix}-G_v^{inv}(s) & -\omega^{ss}C_{inv}\\ \omega^{ss}C_{inv} & -G_v^{inv}(s)\end{bmatrix}$, $\left[B_6\right]_{2\times2}=\begin{bmatrix}K & 0\\ 0 & K\end{bmatrix}$, $\left[B_7\right]_{2\times2}=\begin{bmatrix}0 & G_v^{inv}(s)\\ 0 & 0\end{bmatrix}$.

The small-signal model of (26)-(31) can be shown as:

$$\Delta p_{inv}=1.5\left(V_{cd}\Delta I_{cd}+\Delta V_{cd}I_{cd}+V_{cq}\Delta I_{cq}+\Delta V_{cq}I_{cq}\right) \tag{35}$$

$$\Delta q_{inv}=1.5\left(V_{cd}\Delta I_{cq}+\Delta V_{cd}I_{cq}-V_{cq}\Delta I_{cd}-\Delta V_{cq}I_{cd}\right) \tag{36}$$

$$\Delta\omega=-\frac{m\omega_f}{s+\omega_f}\Delta p_{inv} \tag{37}$$

$$\Delta V_{cd}^{ss}=-\frac{n\omega_f}{s+\omega_f}\Delta q_{inv} \tag{38}$$

Similarly, applying the matrix form on (35)-(38) yields:

$$\begin{bmatrix}\Delta\omega\\ \Delta V_{cd}^{ss}\end{bmatrix}=\left[B_8\right]_{2\times2}\begin{bmatrix}\Delta V_{cd}\\ \Delta V_{cq}\end{bmatrix}+\left[B_9\right]_{2\times2}\begin{bmatrix}\Delta I_{cd}\\ \Delta I_{cq}\end{bmatrix} \tag{39}$$

where $\left[B_8\right]_{2\times2}=\begin{bmatrix}\dfrac{1.5m\omega_f}{s+\omega_f}I_{cd}^{ss} & -\dfrac{1.5m\omega_f}{s+\omega_f}I_{cq}^{ss}\\ -\dfrac{1.5n\omega_f}{s+\omega_f}I_{cq}^{ss} & -\dfrac{1.5n\omega_f}{s+\omega_f}I_{cd}^{ss}\end{bmatrix}$, $\left[B_9\right]_{2\times2}=\begin{bmatrix}-\dfrac{1.5m\omega_f}{s+\omega_f}V_{cd}^{ss} & 0\\ 0 & -\dfrac{1.5n\omega_f}{s+\omega_f}V_{cd}^{ss}\end{bmatrix}$.

Thus, the output impedance matrix of the overall PV is:

$$\begin{aligned}\boldsymbol{Z}_{PVout}=\begin{bmatrix}Z_{PVdd} & Z_{PVdq}\\ Z_{PVqd} & Z_{PVqq}\end{bmatrix}=&\left\{\left[B_5\right]+\left[B_7\right]\left[B_8\right]-\left[B_1\right]\left[B_3\right]-\right.\\ &\left.\left[B_1\right]\left[B_4\right]\left[B_8\right]-\left[B_2\right]\left[B_8\right]\right\}^{-1}\left\{\left[B_1\right]\left[B_4\right]\left[B_9\right]+\right.\\ &\left.\left[B_1\right]+\left[B_2\right]\left[B_9\right]-\left[B_6\right]-\left[B_7\right]\left[B_9\right]\right\}\end{aligned} \tag{40}$$

C. Impedance Model of Main Grid

In the main grid subsystem, L_g and C_g in this sub-section are the main grid impedance and capacitor, respectively; and R_g is the equivalent AC-link resistance. The output and input impedances of the source subsystem can be found as [18]:

$$\boldsymbol{Z}_{gout}=\boldsymbol{Y}_{gin}^{-1}=\begin{bmatrix}Z_{dd} & Z_{dq}\\ Z_{qd} & Z_{qq}\end{bmatrix} \tag{41}$$

D. Overall Impedance Models During Different Operation Modes

According to the analysis on different operation modes in Section II and each subsystem impedance model, the overall impedance models during different operation modes can be obtained as follows:

1) Model 1: $\boldsymbol{Z}_{out}=\boldsymbol{Z}_{gout}$ and $\boldsymbol{Y}_{in}=\boldsymbol{Y}_{PEVin}$
2) Model 2: $\boldsymbol{Z}_{out}=\boldsymbol{Z}_{gout}\ /\!/\ \boldsymbol{Z}_{PVout}$ and $\boldsymbol{Y}_{in}=\boldsymbol{Y}_{PEVin}$
3) Model 3: $\boldsymbol{Z}_{out}=\boldsymbol{Z}_{PVout}$ and $\boldsymbol{Y}_{in}=\boldsymbol{Y}_{PEVin}$
4) Model 4: $\boldsymbol{Z}_{out}=\boldsymbol{Z}_{PVout}$ and $\boldsymbol{Y}_{in}=\boldsymbol{Y}_{PEVin}\ /\!/\ \boldsymbol{Y}_{gin}$

where $\boldsymbol{Z}_{out}$ and $\boldsymbol{Y}_{in}$ are the output impedance matrix of the total source subsystem and the input admittance matrix of the load subsystem, respectively; $\boldsymbol{Y}_{PEVin}$ and $\boldsymbol{Z}_{PVout}$ are the admittance matrix of the overall PEV and the impedance matrix of the overall PV, respectively; and $\boldsymbol{A}\ /\!/\ \boldsymbol{B}$ stands for $\boldsymbol{A}$ and $\boldsymbol{B}$ in parallel.

Remark 1: considering the charging station consisting of multiple PEVs and multiple PVs defined in the Danish EDISON project, $\boldsymbol{Z}_{PVout}=\boldsymbol{Z}_{PVout1}\ /\!/\ \boldsymbol{Z}_{PVout2}\ /\!/\ \cdots\ /\!/\ \boldsymbol{Z}_{PVoutn}$, and n represents the number of the PVs. $\boldsymbol{Y}_{PEVin}=\boldsymbol{Y}_{PEVin1}\ /\!/\ \boldsymbol{Y}_{PEVin2}\ /\!/\ \cdots\ /\!/\ \boldsymbol{Y}_{PEVinm}$, and m represents the number of the PEVs.

E. Impedance-norm-based Stability Criterion

As shown in Fig. 5, the total input-to-output transfer function of the cascade of two individual stable subsystems is:

$$\boldsymbol{G}_{12}=\frac{\boldsymbol{V}_{out,2}}{\boldsymbol{V}_{in,1}}=\boldsymbol{G}_1\frac{\boldsymbol{Z}_{in,2}}{\boldsymbol{Z}_{in,2}+\boldsymbol{Z}_{out,1}}\boldsymbol{G}_2=\boldsymbol{G}_1\frac{1}{1+\boldsymbol{Z}_{out,1}/\boldsymbol{Z}_{in,2}}\boldsymbol{G}_2=\boldsymbol{G}_1\frac{1}{1+\boldsymbol{Z}_{out,1}\boldsymbol{Z}_{in,2}}\boldsymbol{G}_2 \tag{42}$$

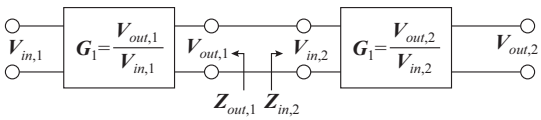

Fig. 5. Interconnection of two stable independent systems.

Since $\boldsymbol{G}_1$ and $\boldsymbol{G}_2$ do not have the right pole, the system is stable if and only if $\boldsymbol{E}+\boldsymbol{Z}_{out,1}\boldsymbol{Y}_{in,2}$ does not have the right pole where $\boldsymbol{E}$ is a unit matrix. In other words, the number of the counterclockwise encirclements of point $(-1+\mathrm{j}0)$ by the ratio between the output impedance of the source-side subsystem and the input impedance of the load-side subsystem locus should be equal to the number of RHP poles of the minor loop gain. In fact, the number of RHP poles is always zero.

As mentioned above, this ratio must not encircle point $(-1+\mathrm{j}0)$ on Nyquist contours. If the eigenvalues of $\boldsymbol{Z}_{out}\boldsymbol{Y}_{in}$ over the all frequency range are restrained inside the unit circle, the stability of the charging station can be guaranteed.

$$\rho\left(\boldsymbol{Z}_{out}\boldsymbol{Y}_{in}\right)<1 \tag{43}$$

$$\boldsymbol{Z}_{out}=\begin{bmatrix}Z_{dd} & Z_{dq}\\ Z_{qd} & Z_{qq}\end{bmatrix} \tag{44}$$

$$\boldsymbol{Y}_{in}=\begin{bmatrix}Y_{dd} & Y_{dq}\\ Y_{qd} & Y_{qq}\end{bmatrix} \tag{45}$$

According to the compatibility and homogeneity of the matrix norm, (43) can be rewritten as:

$$\rho\left(\boldsymbol{Z}_{out}\boldsymbol{Y}_{in}\right)\le\left\|\boldsymbol{Z}_{out}\boldsymbol{Y}_{in}\right\|_A<1 \tag{46}$$

where $\|\cdot\|_A$ is the arbitrarily consistent matrix norm.

Using (44)-(46), we can obtain:

$$\left\|\boldsymbol{Z}_{out}\boldsymbol{Y}_{in}\right\|_A=\begin{Vmatrix}Z_{dd}Y_{dd}+Z_{qd}Y_{qd} & Z_{dd}Y_{dq}+Z_{dq}Y_{qq}\\ Z_{qd}Y_{dd}+Z_{qq}Y_{qd} & Z_{qd}Y_{dq}+Z_{qq}Y_{qq}\end{Vmatrix}<1 \tag{47}$$

To simplify (47), as two kinds of common consistent matrix norms, the infinity norm and the one norm can be chosen, respectively. The charging station is stable if (48) can be satisfied.

$$\min\left(\left\|\boldsymbol{Z}_{out}\boldsymbol{Y}_{in}\right\|_1,\left\|\boldsymbol{Z}_{out}\boldsymbol{Y}_{in}\right\|_\infty\right)<1 \tag{48}$$

Once again, using (47) and (48), the expression of the stability condition can be described as:

$$\begin{aligned}\min\Big[&\max\left(\left|Z_{dd}Y_{dd}+Z_{dq}Y_{qd}\right|+\left|Z_{dd}Y_{dq}+Z_{dq}Y_{qq}\right|,\right.\\&\left.\left|Z_{qd}Y_{dd}+Z_{qq}Y_{qd}\right|+\left|Z_{qd}Y_{dq}+Z_{qq}Y_{qq}\right|\right),\\&\max\left(\left|Z_{dd}Y_{dd}+Z_{dq}Y_{qd}\right|+\left|Z_{qd}Y_{dd}+Z_{qq}Y_{qd}\right|,\right.\\&\left.\left.\left|Z_{dd}Y_{dq}+Z_{dq}Y_{qq}\right|+\left|Z_{qd}Y_{dq}+Z_{qq}Y_{qq}\right|\right)\Big]<1\end{aligned} \tag{49}$$

When the first item is the minimum, (49) is satisfied if:

$$\begin{cases}\left|Z_{dd}Y_{dd}+Z_{dq}Y_{qd}\right|+\left|Z_{dd}Y_{dq}+Z_{dq}Y_{qq}\right|<1\\ \left|Z_{qd}Y_{dd}+Z_{qq}Y_{qd}\right|+\left|Z_{qd}Y_{dq}+Z_{qq}Y_{qq}\right|<1\end{cases} \tag{50}$$

Moreover, the sufficient condition satisfying (50) is gained through (51), which can be switched to (52) further.

$$\begin{cases}\left|Z_{dd}\right|\left|Y_{dd}\right|+\left|Z_{dq}\right|\left|Y_{qd}\right|+\left|Z_{dd}\right|\left|Y_{dq}\right|+\left|Z_{dq}\right|\left|Y_{qq}\right|<1\\ \left|Z_{qd}\right|\left|Y_{dd}\right|+\left|Z_{qq}\right|\left|Y_{qd}\right|+\left|Z_{qd}\right|\left|Y_{dq}\right|+\left|Z_{qq}\right|\left|Y_{qq}\right|<1\end{cases} \tag{51}$$

$$\begin{cases}\left|Z_{dd}\right|\left(\left|Y_{dd}\right|+\left|Y_{dq}\right|\right)+\left|Z_{dq}\right|\left(\left|Y_{qd}\right|+\left|Y_{qq}\right|\right)<1\\ \left|Z_{qd}\right|\left(\left|Y_{dd}\right|+\left|Y_{dq}\right|\right)+\left|Z_{qq}\right|\left(\left|Y_{qd}\right|+\left|Y_{qq}\right|\right)<1\end{cases} \tag{52}$$

Furthermore, (53) can be met if:

$$\begin{cases}\left(\left|Z_{dd}\right|+\left|Z_{dq}\right|\right)\max\left\{\left(\left|Y_{dd}\right|+\left|Y_{dq}\right|\right),\left(\left|Y_{qd}\right|+\left|Y_{qq}\right|\right)\right\}<1\\ \left(\left|Z_{qd}\right|+\left|Z_{qq}\right|\right)\max\left\{\left(\left|Y_{dd}\right|+\left|Y_{dq}\right|\right),\left(\left|Y_{qd}\right|+\left|Y_{qq}\right|\right)\right\}<1\end{cases} \tag{53}$$

Moreover, the sufficient condition that satisfies (54) can be derived as:

$$\begin{aligned}&\max\left\{\left(\left|Z_{dd}\right|+\left|Z_{dq}\right|\right),\left(\left|Z_{qd}\right|+\left|Z_{qq}\right|\right)\right\}\times\\&\max\left\{\left(\left|Y_{dd}\right|+\left|Y_{dq}\right|\right),\left(\left|Y_{qd}\right|+\left|Y_{qq}\right|\right)\right\}<1\end{aligned} \tag{54}$$

On the basis of (55), this condition could be expressed by the matrix infinity norms of $Z_{out}(s)$ and $Y_{in}(s)$:

$$\left\|\boldsymbol{Z}_{out}(s)\right\|_\infty\left\|\boldsymbol{Y}_{in}(s)\right\|_\infty<1 \tag{55}$$

When the second item is the minimum, a similar analysis is utilized to analyze the stability condition of the charging station.

$$\begin{cases}\left|Z_{dd}Y_{dd}+Z_{dq}Y_{qd}\right|+\left|Z_{qd}Y_{dd}+Z_{qq}Y_{qd}\right|<1\\ \left|Z_{dd}Y_{dq}+Z_{dq}Y_{qq}\right|+\left|Z_{qd}Y_{dq}+Z_{qq}Y_{qq}\right|<1\end{cases} \tag{56}$$

Moreover, (56) is satisfied if (57) can be met, which can be switched to (58) further.

$$\begin{cases}\left|Z_{dd}\right|\left|Y_{dd}\right|+\left|Z_{dq}\right|\left|Y_{qd}\right|+\left|Z_{qd}\right|\left|Y_{dd}\right|+\left|Z_{qq}\right|\left|Y_{qd}\right|<1\\ \left|Z_{dd}\right|\left|Y_{dq}\right|+\left|Z_{dq}\right|\left|Y_{qq}\right|+\left|Z_{qd}\right|\left|Y_{dq}\right|+\left|Z_{qq}\right|\left|Y_{qq}\right|<1\end{cases} \tag{57}$$

$$\begin{cases}\left(\left|Z_{dd}\right|+\left|Z_{qd}\right|\right)\left|Y_{dd}\right|+\left(\left|Z_{dq}\right|+\left|Z_{qq}\right|\right)\left|Y_{qd}\right|<1\\ \left(\left|Z_{dd}\right|+\left|Z_{qd}\right|\right)\left|Y_{dq}\right|+\left(\left|Z_{dq}\right|+\left|Z_{qq}\right|\right)\left|Y_{qq}\right|<1\end{cases} \tag{58}$$

Additionally, (58) can be met if the following inequality is satisfied:

$$\begin{cases}\max\left\{\left(\left|Z_{dd}\right|+\left|Z_{qd}\right|\right),\left(\left|Z_{dq}\right|+\left|Z_{qq}\right|\right)\right\}\left(\left|Y_{dd}\right|+\left|Y_{qd}\right|\right)<1\\ \max\left\{\left(\left|Z_{dd}\right|+\left|Z_{qd}\right|\right),\left(\left|Z_{dq}\right|+\left|Z_{qq}\right|\right)\right\}\left(\left|Y_{dq}\right|+\left|Y_{qq}\right|\right)<1\end{cases} \tag{59}$$

Further, (59) is met if the following inequality is satisfied:

$$\begin{aligned}&\max\left\{\left(\left|Z_{dd}\right|+\left|Z_{qd}\right|\right),\left(\left|Z_{dq}\right|+\left|Z_{qq}\right|\right)\right\}\times\\&\max\left\{\left(\left|Y_{dd}\right|+\left|Y_{qd}\right|\right),\left(\left|Y_{dq}\right|+\left|Y_{qq}\right|\right)\right\}<1\end{aligned} \tag{60}$$

According to (60), the sufficient condition of the stability

assessment could be obtained through the one-norms of $\boldsymbol{Z}_{out}(s)$ and $\boldsymbol{Y}_{in}(s)$:

$$\left\|\boldsymbol{Z}_{out}(s)\right\|_1 \left\|\boldsymbol{Y}_{in}(s)\right\|_1 < 1 \tag{61}$$

To sum up, when each subsystem is stable independently, the sufficient condition to judge the system stability is that (62) is satisfied. In other words, the system must be stable if the minimum value between the arithmetic product of the matrix infinity norms of the source subsystem output impedance $\boldsymbol{Z}_{out}(s)$ as well as the load subsystem input admittance $\boldsymbol{Y}_{in}(s)$ and arithmetic product of the one-norms of the source subsystem output impedance $\boldsymbol{Z}_{out}(s)$ as well as the load subsystem input admittance $\boldsymbol{Y}_{in}(s)$ is less than one.

$$\min\left(\left\|\boldsymbol{Z}_{out}(s)\right\|_\infty \left\|\boldsymbol{Y}_{in}(s)\right\|_\infty, \left\|\boldsymbol{Z}_{out}(s)\right\|_1 \left\|\boldsymbol{Y}_{in}(s)\right\|_1\right) < 1 \tag{62}$$

Apparently, the conservatism of the MION criterion is less than the IN criterion whose conservatism is less than other norm criteria [18]. Thus, the MION criterion has minimum conservatism among the above-mentioned norm criteria.

Remark 2: the detailed stability assessment of AC-bus bar for the PEV charging station with PV is provided as follows.

Step 1: the stability of each subsystem should be identified through the previous literatures [4], [12], which has been widely Studied. If the stability of each subsystem is ensured, then go to *Step 2*. Note that this step is not an important studied object in this paper, and this paper focuses more on the interactive stability, i.e., *Step 2*.

Step 2: the stability of the complex system is identified through the proposed MION stability criterion. If the (62) is satisfied, the AC-busbar PEV charging station with PV must be stable.

F. Stability Analysis of AC-busbar PEV Charging Station with PV

As mentioned above, the stability of the AC-busbar PEV charging station with PV in electromagnetic timescale can be ensured that every PV and PEV in the charging station is stable, and that the MION stability criterion is satisfied.

In order to ensure the stability of each PV and PEV, the subsystem parameters can be designed as follows. Firstly, the stability analysis of each PV and PEV has been widely studied. The control bandwidth of the inner-loop voltage controller is around 5 times lower than that of the inner-loop current controller, which satisfies the standard bandwidth ratio design criterion. Under this effect, converter is prone to operating stably. Thus, the stability of the inner voltage and current controller can be ensured in advance by tuning their bandwidth to satisfy the standard bandwidth ratio design criterion [24]. Furthermore, the PLL controller parameters can be represented in light of ω_n and ζ, where $k_p^{PLL}=2\zeta\omega_n$ and $k_i^{PLL}=\omega_n^2$. The natural frequency ω_n can be chosen as the indicator of the PLL bandwidth, and ζ is the damping factor [25]. Eventually, the smaller the droop coefficient bandwidth is, the better the converter stability will be. But the converter dynamic response will be slower accordingly. Thus, there is a trade between stability and dynamic response [26].

From the viewpoint of the MION stability criterion, as shown in (62), the smaller $\boldsymbol{Z}_{out}$ is and the larger $\boldsymbol{Y}_{in}$ is, the better the charging station stability will be. At present, the charging station is mainly located in remote areas, and it is weakly connected to the main grid with high impedance, i.e., the SCR of the main grid is small. Thus, the instability phenomenon of the AC-busbar PEV charging station with PV is prone to occurring in Mode 1. Furthermore, with the increase of PEVs, the stability of the charging station will be reduced, which is likely to result in the instability phenomenon of the charging station in Mode 4. In order to deal with this instability problem, it is possible to design a suitable source impedance which should be adapted to a certain range of load impedance variation. Meanwhile, the doubly-fed line and energy storage equipment connected in parallel with the main grid will be two advisable choices. The aim is to reduce the output impedance of the source subsystem $\boldsymbol{Z}_{out}$.

Remark 3: the studied system in this paper can be regarded as the weak grid with various loads. The interaction between the weak grid and load always causes instability issues and low-frequency or harmonic oscillation in the real applications. Furthermore, the weak grid is becoming increasingly complex, incorporating distributed renewable energy sources, various loads, etc. For studying the stability issue of the cascaded system, SCR is widely utilized to assess the strength of the cascaded system, and the weak grid is further emulated through the ideal voltage source in series with one-line impedance [27]. Therein, the doubly-fed line and energy storage equipment are always connected to the weak grid to enhance its strength. In other words, these operations are able to increase the SCR of weak grids. The relationship among grid strength, SCR and equivalent line impedance can be shown in Fig. 6.

Fig. 6. Relationship among grid strength, SCR and line impedance.

To sum up, the equivalent impedance of the main grid can be reduced through connecting the doubly-fed line and energy storage equipment. Meanwhile, the selection rule can be provided. The strength of the grid is distinguished by SCR ($SCR=S_{SC}/S_N$) [28], where S_{SC} is the short-circuit capacity at the PCC, and S_N is the rated capacity of the grid-connected equipment. Generally, a grid is considered strong for SCR above 20 to 25, weak for SCR below 6 to 10 and ultra-weak for SCR below 2 [28]. First and foremost, the desired equivalent line impedance is obtained through the proposed stability criterion. Furthermore, the relative SCR can be given in [27]. Eventually, according to the desired SCR, the detailed specifications of the doubly-fed line and energy storage equipment can be selected through professional power system designers.

IV. Simulation

To verify the effectiveness and conservatism of the impedance-norm-based stability criterion for the AC-busbar PEV charging station with PV, the voltage and frequency in the simulation system are selected as the standard voltage and frequency of the power system in China. The system consists of one PEV, one PV, and the main grid, as depicted in

Fig. 2. Since this paper focuses on the interactive stability, the stability of each subsystem should be ensured in advance. In this section, the relative parameters are selected to guarantee two condition as follows: ① the PEV and main grid are stable when supplied by an ideal voltage source; ② the main-gird itself and PV are stable when unload, i. e., when the load is an open circuit. In order to satisfy the aforementioned conditions, the control parameters of the interfaced converter are the same as those in the previous literature where the subsystem stability is ensured. Therein, the parameters of the PEV are the same as those in [18], and the parameters of the PV are the same as those in [29]. Additionally, this instability phenomenon caused by impedance mismatching has been widely reported [30], [31].

A. Conservatism

To verify conservatism of the proposed MION stability criterion based on the impedance approach, the tested system can be obtained in Model 1. Therein, $G_{PLL} = 0.58 + 10/s$, $L_{rec} = 10$ mH, and main grid impedance is $L_g = 0.8$ mH, $C_g = 10$ mF, $R_g = 0.11$ Ω, $C_{dc} = 20$ mF, and $R_{load} = 10$ Ω. First and foremost, it can be seen from Fig. 7(a) that the MION is less than one from 0 to 10000 Hz. However, the GN is larger than 0.25 from 13 Hz to 203 Hz, the ION is larger than 0.5 from 14 Hz to 134 Hz, and the IN is larger than one from 28 Hz to 47 Hz. Thus, the MION criterion is satisfied, whilst the GN, ION and IN criteria are not met. According to the MION criterion, the charging station is stable, whilst it is possible that the charging station will be unstable due to the GN, ION and IN criteria. The stability of charging station could be clearly identified by testing the time-domain waveforms for checking the conclusion of stability criteria.

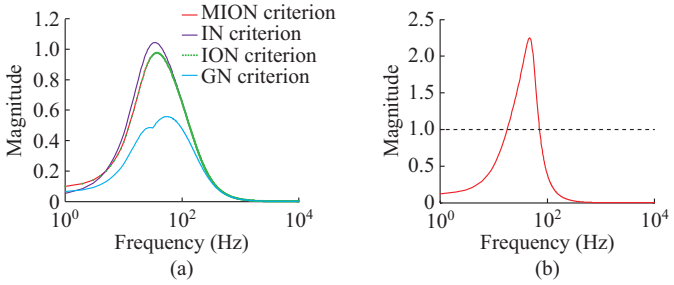

Fig. 7. Stability criteria. (a) Results of several stability criteria at the beginning of operation Mode 1. (b) Results of MION criterion when main grid resistance is changed.

In Fig. 8(a), the AC-busbar voltage is in accordance with the conclusion assessed by the proposed MION criterion, whereas it is not in accordance with the result assessed by the other criteria. Compared with the heretofore available criteria, the conservatism of the MION criterion is greatly reduced. Meanwhile, the effectiveness of the MION stability criterion can also be verified. The only main grid resistance is increased to $R_g = 1$ Ω. It is shown in Fig. 7(b) that the MION is larger than one from 18 Hz to 72 Hz. Therefore, it is possible that the simulation system will be unstable according to the MION criterion. The stability of the charging station can be clearly verified by testing the time-domain waveforms. Apparently, the simulation system is unstable as shown in Fig. 8(b) where the AC-side voltage is in accordance with the instability phenomenon. Therein, this instability is caused by improper selection of the line impedance parameter. Thus, the effectiveness of the proposed MION criterion can be verified.

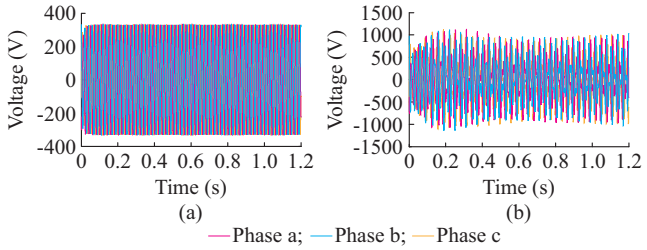

Fig. 8. AC-busbar voltage time-domain waveforms. (a) Simulation results at the beginning of operation Mode 1. (b) Simulation results when main grid resistance is changed.

B. Effectiveness

To verify the effectiveness of the impedance-norm-based stability criterion for the AC-busbar PEV charging station with PV and the stability recovery way, the different modes can be analyzed by testing the time-domain waveforms. In this subsection, the parameters of the PV are given as follows. The droop coefficients are $m = 2 \times 10^{-6}$ and $n = 3.4 \times 10^{-4}$, respectively; the double-loop current and voltage controllers are $G_v^{inv} = 1 + 8/s$ and $G_i^{inv} = 4 + 150/s$, respectively. Meanwhile, the parameters of the PEV are shown as follows: $G_{PLL} = 180 + 3200/s$; and the double-loop current and voltage controllers are $G_v^{rec} = 0.5 + 5/s$, $G_i^{rec} = 3 + 100/s$, respectively. Furthermore, the main grid impedance is $L_g = 10$ mH, $C_g = 1$ mF, $R_g = 1$ Ω, whose value is different from that in the Section IV-A. It can be seen from Fig. 9(a) that the MION is larger than one from 23.5 to 87 Hz in Mode 1, and is larger than one from 35 to 39 Hz in Mode 4. The MION is, however, less than one from 0 to 10000 Hz in Mode 2 or 3. Thus, it is possible that the simulation system will be unstable in Mode 1 or 4. As shown in Fig. 10(a) and (d), the AC-busbar PEV charging station with PV is unstable in Mode 1 or 4 where the AC-side voltage is in accordance with the instability phenomenon. Meanwhile, It can be shown in Fig. 10(b) and (c) that the AC-busbar voltage is in accordance with the conclusion proposed MION criterion. Thus, the effectiveness of the proposed MION criterion can be verified. In order to make the charging station stable, the doubly-fed line and energy storage equipment connected in parallel with the main grid can be applied to reduce the impedance of the main grid. Thus, the impedance is increased to $L_g = 10$ mH, $C_g = 100$ μF, $R_g = 0.11$ Ω. It can be seen from Fig. 10(b) that the MION is less than one from 0 to 10000 Hz in Mode 1 to Mode 4. The stability of the charging station can be clearly verified by testing the time-domain waveforms. The simulation system is stable as shown in Fig. 11, where the AC-side voltage is in accordance with the stability phenomenon. Note that the voltage magnitude is 311 V in the stable condition, whereas the voltage magnitude exceeds 1000 V in the unstable condition. If the vertical and horizontal axes in all figures are set to the same value, the voltage time-waveforms in the stable condition are not clear

and so small. Based on this, the vertical and horizontal axes in the relative figures are different. To sum up, the effectiveness of the proposed MION criterion can be verified.

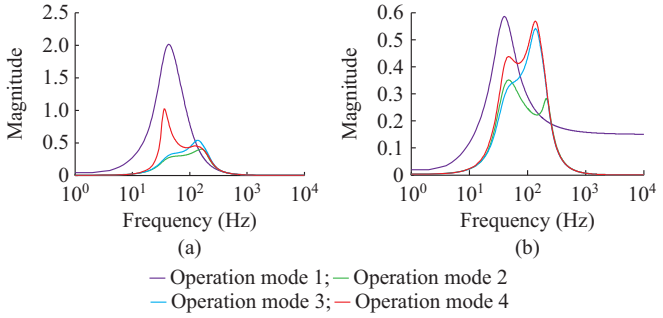

Fig. 9. Results of proposed MION stability criterion in different operation modes. (a) MION criterion results at the beginning of different operation modes. (b) MION criterion results of different operation modes when main grid impedance is changed.

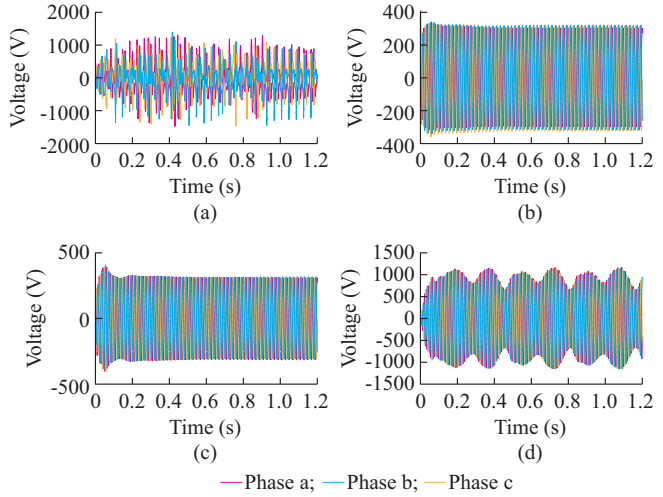

Fig. 10. AC-busbar voltage time-domain waveforms at the beginning of different operation modes. (a) Time-domain waveform in operation Mode 1. (b) Time-domain waveform in operation Mode 2. (c) Time-domain waveform in operation Mode 3. (d) Time-domain waveform in operation Mode 4.

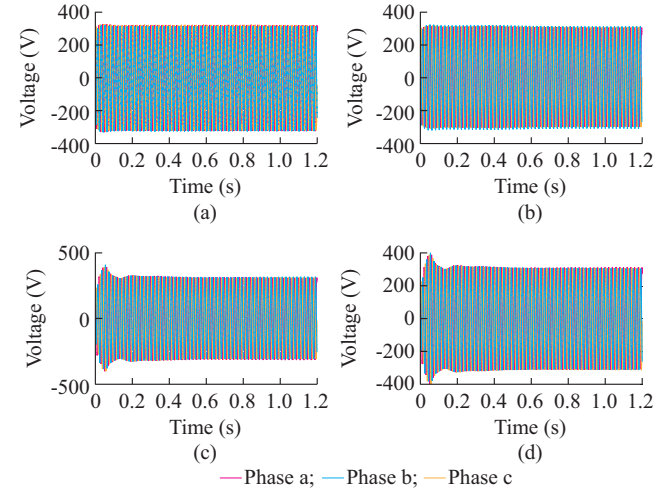

Fig. 11. AC-busbar voltage time-domain waveforms when main grid impedance is changed. (a) Time-domain waveform in operation Mode 1. (b) Time-domain waveform in operation Mode 2. (c) Time-domain waveform in operation Mode 3. (d) Time-domain waveform in operation Mode 4.

V. Experiment

A 4.4 V, 50 Hz AC-busbar PEV charging station with PV is built to verify the effectiveness of the proposed approach. As shown in Fig. 3, the test system consists of an equivalent PV (one PV generator and one three-phase inverter), an equivalent PEV (one battery and one rectifier), and the main grid (one adjustable mutual inductor and the three-phase AC main grid). The system switch frequency is 19.2 kHz.

In order to verify the performances of the proposed stability criterion and the stability recovery way, the different modes can be analyzed by testing the time-domain waveforms, which is similar with the previous section. In this section, the parameters of the PV are shown as follows: the droop coefficients are $m=2\times10^{-5}$ and $n=3.4\times10^{-3}$, respectively; and the other parameters are same as that in the simulation. Furthermore, the main grid impedance is L_g = 10 mH, $C_g=1$ mF, R_g = 0.1 Ω.

It can be seen from Fig. 12(a) that the MION is larger than one from 20 Hz to 344 Hz in Mode 1, and is larger than one from 33 Hz to 42 Hz in Mode 4. The MION is, nevertheless, less than one from 0 to 10000 Hz in Mode 2 or 3. Thus, it is possible that the simulation system will be unstable in Mode 1 or 4. As shown in Fig. 13(a) and (d), the AC-busbar PEV charging station with PV is unstable in Mode 1 or 4. Meanwhile, it can be shown in Fig. 13(b) and (c) that the AC-bus voltage is in accordance with the conclusion obtained by MION criterion. Thus, the effectiveness of the proposed MION criterion can be verified. In order to make the charging station stable, the doubly-fed line and energy storage equipment connected in parallel with the main grid can be applied to reduce the main grid impedance. If the main grid impedance is changed to L_g = 1 mH, $C_g=100$ μF, R_g = 0.1 Ω, the MION is less than one from 0 to 10000 Hz in Mode 1 to Mode 4, which is shown in Fig. 12(b). The stability of the charging station can be clearly verified by testing the time-domain waveforms. The experimental system is stable, which is shown in Fig. 14. According to the aforementioned experimental results shown in Figs. 13 and 14, the proposed stability criterion can identify the stability of the AC-busbar PEV charging station with PV. Thus, the effectiveness of the proposed MION criterion and stability way recovery can be verified.

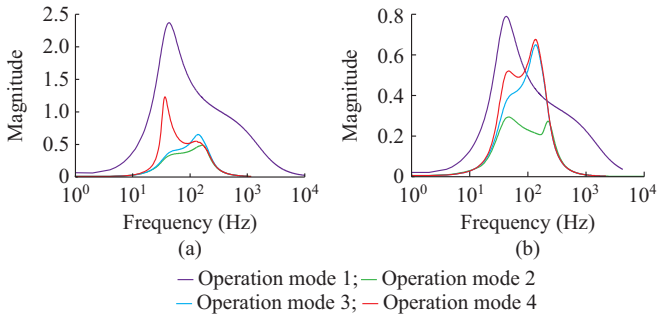

Fig. 12. Proposed MION stability criterion results in experiment test system. (a) MION criterion results at the beginning of different operation modes. (b) MION criterion results of different operation modes when main grid impedance is changed.

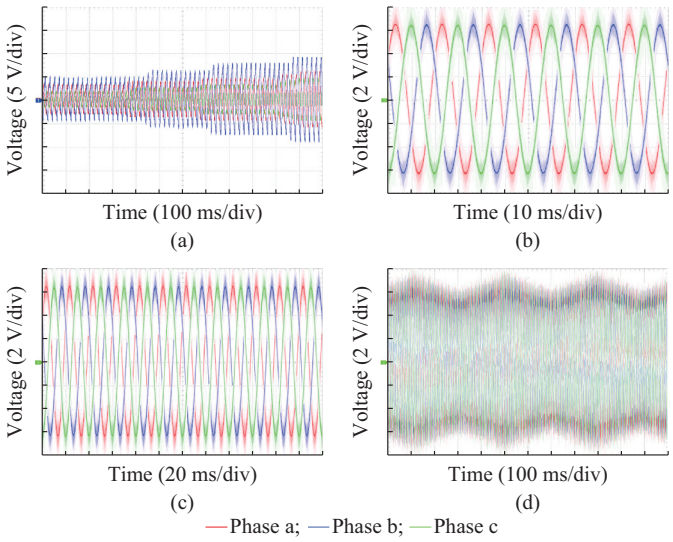

Fig. 13. AC-bus voltage time-domain waveforms. (a) Operation Mode 1. (b) Operation Mode 2. (c) Operation Mode 3. (d) Operation Mode 4.

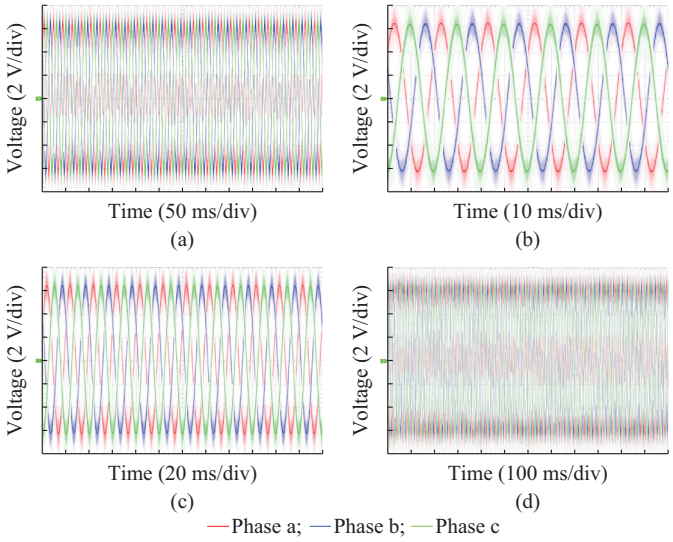

Fig. 14. AC-bus voltage time-domain waveforms when main grid impedance is changed. (a) Operation Mode 1. (b) Operation Mode 2. (c) Operation Mode 3. (d) Operation Mode 4.

Remark 4: To verify that the proposed MION stability criterion can be applied to the real system, the voltage and frequency in the simulation system are selected as the standard voltage and frequency of the power system in China. Unfortunately, the same voltage and frequency cannot be chosen in the experiment system due to our current hardware conditions. Therefore, the low-voltage experiment system is provided to verify the performance of the proposed stability criterion. Of course, the same parameters in both simulation and experiment system are important, and we will try our best to improve our hardware conditions in the future.

VI. Conclusion

Although the AC-busbar PEV charging station with PV has become an attractive choice to reduce fuel consumption and CO2 emissions, the interaction among the main grid, PEVs and PVs always causes the instability problem. Besides, the conventional GNC is complex, and it is not suitable for the design of the AC system. Based on these, this paper has proposed an MION stability criterion based on the impedance method to assess the stability of the AC-busbar PEV charging station with PV. Through theoretical analysis, simulation and experimental results, the proposed stability criterion can be used to assess the studied system stability. Furthermore, compared with the relatively simplified stability criteria in [18] and [19], the proposed stability criterion has lower conservatism through simulation and experimental results. Meanwhile, the effectiveness of the stability recovery way has been verified through simulation and experimental results.

Appendix A

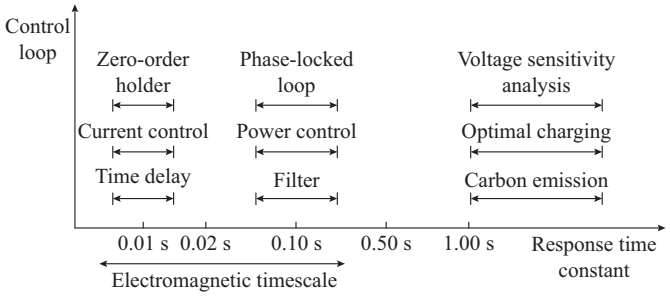

Fig. AI. Extending classification of multi-timescale.

TABLE AI
Styles of Norm Criterion

Norm criterion style	Stability condition
GN criterion [19]	$\left\|\boldsymbol{Z}_{out}\right\|_G\left\|\boldsymbol{Y}_{in}\right\|_G<0.25, \omega\subseteq(-\infty+\infty)$ $\left\|\boldsymbol{A}_{m\times n}\right\|_G=\max_{\substack{1\le i\le m\\1\le j\le n}}\left(\left\|a_{ij}\right\|\right)$, where n and m are the matrix dimension
Infinity-one-norm criterion [19]	$\left\|\boldsymbol{Z}_{out}\right\|_\infty\left\|\boldsymbol{Y}_{in}\right\|_1<0.5, \omega\subseteq(-\infty+\infty)$ $\left\|\boldsymbol{A}_{m\times n}\right\|_\infty=\max_{1\le i\le m}\left(\sum_{j=1}^{n}\left\|a_{ij}\right\|\right)$ $\left\|\boldsymbol{A}_{m\times n}\right\|_1=\max_{1\le j\le n}\left(\sum_{i=1}^{m}\left\|a_{ij}\right\|\right)$
Infinity-norm criterion [18]	$\left\|\boldsymbol{Z}_{out}\right\|_\infty\left\|\boldsymbol{Y}_{in}\right\|_\infty<1, \omega\subseteq(-\infty+\infty)$ $\left\|\boldsymbol{A}_{m\times n}\right\|_\infty=\max_{1\le i\le m}\left(\sum_{j=1}^{n}\left\|a_{ij}\right\|\right)$

References

[1] H. Cheng, L. Wang, L. Xu *et al.*, "An integrated electrified powertrain topology with SRG and SRM for plug-in hybrid electrical vehicle," *IEEE Transactions on Industrial Electronics*, vol. 67, no. 10, pp. 8231-8241, Oct. 2020.

[2] R. Wang, Q. Sun, P. Zhang *et al.*, "Reduced-order transfer function model of the droop-controlled inverter via jordan continued-fraction expansion," *IEEE Transactions on Energy Conversion*, vol. 35, no. 3, pp. 1585-1595, Mar. 2020.

[3] F. Marra, "Central station design options," Department of Electrical Engineering, Technical University of Denmark, Tech. Rep. D4.1, Dec. 2011.

[4] R. Wang, Q. Sun, D. Ma *et al.*, "The small-signal stability analysis of the droop-controlled converter in electromagnetic timescale," *IEEE Transactions on Sustainable Energy*, vol. 10, no. 3, pp. 1459-1469,

Jul. 2019.
[5] H. Yuan, X. Yuan, and J. Hu, "Modeling of grid-connected VSCs for power system small-signal stability analysis in DC-link voltage control timescale," *IEEE Transactions on Power Systems*, vol. 32, no. 5, pp. 3981-3991, Sept. 2017.
[6] N. Liu, Q. Chen, J. Liu *et al*., "A heuristic operation strategy for commercial building microgrids containing EVs and PV system," *IEEE Transactions on Industrial Electronics*, vol. 62, no. 4, pp. 2560-2570, Apr. 2015.
[7] Y. Li, D. Gao, W. Gao *et al*., "Double-mode energy management for multi-energy system via distributed dynamic event-triggered Newton-Raphson algorithm," *IEEE Transactions on Smart Grid*, doi: 10.1109/TSG.2020.3005179.
[8] D. Said and H. T. Mouftah, "A novel electric vehicles charging/discharging management protocol based on queuing model," *IEEE Transactions on Intelligent Vehicles*, vol. 5, no. 1, pp. 100-111, Mar. 2020.
[9] X. Zhang, X. Ruan, and C. K. Tse, "Impedance-based local stability criterion for DC distributed power systems," *IEEE Transactions on Circuits and Systems*, vol. 62, no. 3, pp. 916-925, Mar. 2015.
[10] E. A. A. Coelho, P. C. Cortizo, and P. F. D. Garcia, "Small-signal stability for parallel-connected inverters in stand-alone AC supply systems," *IEEE Transactions on Industry Applications*, vol. 38, no. 2, pp. 533-542, Mar. 2002.
[11] N. Pogaku, M. Prodanovic, and T. C. Green, "Modeling, analysis and testing of autonomous operation of an inverter-based microgrid," *IEEE Transactions on Power Electronics*, vol. 22, no. 2, pp. 613-625, Mar. 2007.
[12] M. Rasheduzzaman, J. A. Mueller, and J. W. Kimball, "Reduced order small-signal model of microgrid systems," *IEEE Transactions on Sustainable Energy*, vol. 6, no. 4, pp. 1292-1305, Oct. 2015.
[13] Y. Wang, X. Wang, F. Blaabjerg *et al*., "Harmonic instability assessment using state-space modeling and participation analysis in inverter-fed power systems," *IEEE Transactions on Industrial Electronics*, vol. 64, no. 1, pp. 806-816, Jan. 2017.
[14] A. A. A. Radwan and Y. A. I. Mohamed, "Analysis and active impedance-based stabilization of voltage-source-rectifier loads in grid-connected and isolated microgrid applications," *IEEE Transactions on Sustainable Energy*, vol. 4, no. 3, pp. 563-576, Jul. 2013.
[15] B. Wen, D. Boroyevich, R. Burgos *et al*., "Inverse Nyquist stability criterion for grid-tied inverters," *IEEE Transactions on Power Electronics*, vol. 32, no. 2, pp. 1548-1556, Feb. 2017.
[16] F. Liu, J. Liu, H. Zhang *et al*., "Stability issues of $Z + Z$ type cascade system in hybrid energy storage system (HESS)," *IEEE Transactions on Power Electronics*, vol. 29, no. 11, pp. 5846-5859, Nov. 2014.
[17] M. Amin, M. Molinas, J. Lyu *et al*., "Impact of power flow direction on the stability of VSC-HVDC seen from the impedance Nyquist plot," *IEEE Transactions on Power Electronics*, vol. 32, no. 10, pp. 8204-8217, Oct. 2017.
[18] Z. Liu, J. Liu, W. Bao *et al*., "Infinity-norm of impedance-based stability criterion for three-phase AC distributed power systems with constant power loads," *IEEE Transactions on Power Electronics*, vol. 30, no. 6, pp. 3030-3043, Jun. 2015.
[19] M. Belkhayat, "Stability criterion for AC power systems with regulated loads," Ph.D. dissertation, Department of Electrical and Computer Engineering, Purdue University, West Lafayette, USA, 1997.
[20] H. Mao, D. Boroyevich, and F. C. Lee, "Novel reduced-order small signal model of a three-phase PWM rectifier and its application in control design and system analysis," *IEEE Transactions on Power Electronics*, vol. 13, no. 3, pp. 511-521, May 1998.
[21] S. Hiti, V. Vlatkovic, D. Boroyevich *et al*., "A new control algorithm for three-phase PWM buck rectifier with input displacement factor compensation," *IEEE Transactions on Power Electronics*, vol. 9, no. 2, pp. 173-180, Mar. 1994.
[22] L. Liu, Y. Liu, S. Tong *et al*., "Integral barrier Lyapunov function based adaptive control for switched nonlinear systems," *Science China - Information Sciences*, vol. 63, no. 3, pp. 1-14, Mar. 2020.
[23] W. Hu, C. Ruan, H. Nian *et al*., "Zero-sequence current suppression strategy with common mode voltage control for open-end winding PMSM drives with common DC bus," *IEEE Transactions on Industrial Electronics*, doi: 10.1109/TIE. 2020. 2988221.
[24] M. Amin and M. Molinas, "A grey-box method for stability and controller parameter estimation in HVDC-connected wind farms based on non-parametric impedance," *IEEE Transactions on Industrial Electronics*, vol. 66, no. 3, pp. 1872-1882, Mar. 2019.
[25] D. Dong, I. Cvetkovic, D. Boroyevich *et al*., "Grid-interface bidirectional converter for residential DC distribution systems, Part I: high-density two-stage topology," *IEEE Transactions on Power Electronics*, vol. 28, no. 4, pp. 1655-1666, Apr. 2013.
[26] R. Wang, Q. Sun, Y. Gui *et al*., "Exponential-function-based droop control for islanded microgrids," *Journal of Modern Power Systems and Clean Energy*, vol. 7, no. 4, pp. 2453-2467, Jul. 2019.
[27] W. Wu, Y. Chen, L. Zhou *et al*., "Sequence impedance modeling and stability comparative analysis of voltage-controlled VSGs and current-controlled VSGs," *IEEE Transactions on Industrial Electronics*, vol. 66, no. 8, pp. 6460-6472, Aug. 2019.
[28] X. Wang and F. Blaabjerg, "Harmonic stability in power electronic based power systems: concept, modeling, and analysis," *IEEE Transactions on Smart Grid*, vol. 10, no. 3, pp. 2858-2870, May 2019.
[29] M. Amin and M. Molinas, "Small-signal stability assessment of power electronics based power systems: a discussion of impedance- and eigenvalue-based methods," *IEEE Transactions on Industrial Applications*, vol. 53, no. 5, pp. 5014-5030, Sept. 2017.
[30] R. Wang, Q. Sun, D. Ma *et al*., "Line impedance cooperative stability region identification method for grid-tied inverters under weak grids," *IEEE Transactions on Smart Grid*, vol. 11, no .4, pp. 2856-2866, Jul. 2020.
[31] W. Cao, Y. Ma, L. Yang *et al.*, "*d-q* impedance based stability analysis and parameter design of three phase inverter-based AC power systems," *IEEE Transactions on Industrial Electronics*, vol. 64, no. 7, pp. 6017-6028, Jul. 2017.

Rui Wang received the B.S. degree in Northeastern University, Shenyang, China, in 2016. He is currently pursuing the Ph.D. degree in the School of Information Science and Engineering, Institute of Automation, Northeastern University, Shenyang, China. Since 2019, he has become a visiting scholar with the Energy Research Institute, Nanyang Technological University, Singapore, Singapore. He has authored or coauthored over 30 papers, authorized over 10 invention patents. His current research interests include collaborative optimization of distributed generation and its stability analysis of electromagnetic timescale in Energy Internet.

Qiuye Sun received the Ph. D. degree from Northearstern University, Shenyang, China, in 2007. He is currently a full Professor with Northeastern University, and obtained Special Government Allowances from the State Council in China. He has authored or coauthored over 200 papers, authorized over 100 invention patents, and published over 10 books or textbooks. His current research interests include optimization analysis technology of power distribution network, network control of energy internet, integrated energy systems and microgrids.

Dehao Qin received the B.S. and M.Sc. degrees in Northeastern University, Shenyang, China, in 2017 and 2020, respectively. He is currently pursuing the Ph.D. degree in the College of Engineering, Computing and Applied Sciences, Clemson University, Clemson, USA. His current research interest includes collaborative control strategy of distributed generation in Energy Internet.

Yushuai Li received the B.S. degree in electrical engineering and automation, and the Ph.D. degree in control theory and control engineering from the Northeastern University, Shenyang, China, in 2014 and 2019, respectively. He is currently a postdoctoral research scholar in the Department of Electrical and Computer Engineering, University of Denver, Denver, USA. His current research interests include distributed control and optimization, machine learning with applications in microgrids, smart grid and energy internet.

Xiangke Li received the B. Eng. degree in Electrical Engineering from Northwestern Polytechnical University, Xi'an, China, in 2016, where he is currently working toward the Ph.D. degree in electrical engineering at the School of Automation. Since 2018, he has become a visiting scholar with the Energy Research Institute, Nanyang Technological University, Singapore. His research interests include modeling, design and control of switched-capacitor converters, distributed generations and microgrids.

Peng Wang received the B.Sc. degree in electronic engineering from Xi'an Jiaotong University, Xi'an, China, in 1978, the M.Sc. degree from Taiyuan University of Technology, Taiyuan, China, in 1987, and the M.Sc. and Ph.D. degrees in electrical engineering from the University of Saskatchewan, Saskatoon, Canada, in 1995 and 1998, respectively. Currently, he is a full Professor with the School of Electrical and Electronic Engineering at Nanyang Technological University, Singapore. His current research interests include power system planning and operation, renewable energy planning, solar/electricity conversion system and power system reliability analysis.